Tendon Locking for Antagonistic Configuration- and Stiffness-Control in Soft Robots

Johann Licher[1,2], Jan Peters[2], Annika Raatz[2], Helge A. Wurdemann[1]

***Abstract*— Some applications, such as surgical interventions, require that potential soft robots have the capability to alter their shape and enhance their force output on demand. This paper presents an antagonistic stiffening mechanism combining pneumatic actuation with tendon locking to achieve configuration- and stiffness control. Elongation of a soft pneumatic section, resulting from air actuation, is opposed by constraining the length of integrated tendons. These tendons can be locked in length by pneumatically activated levers at the base of each segment. Hence, tendon locking will not affect the configuration of other segments of a multi-segment manipulator. Our concept achieves a stiffness increase of up to 201.7 % and a larger, more uniform radial workspace compared to the widely used pneumatic actuation concept while maintaining the low technical effort required for actuation. We also demonstrate how our actuation concept enables independent control of stiffness levels for individual segments of a multi-segment manipulator and their MR compatibility.**

I. Introduction

In applications where traditional rigid robots encounter challenges such as navigating narrow or winding passageways, or requiring inherent safety, soft robots have demonstrated advantages due to their high dexterity and compliance [1]. This has led to a rapid growth in the field of soft material robotics over the past decades [2]. However, a fundamental research question concerns how soft robots can achieve on-demand forces, either through configuration-dependent stiffness analysis and control of manipulators [3] or variable stiffness mechanisms [4]. The integration of variable stiffness mechanisms can, in fact, introduce a significant variation in force exertion, but is also associated with challenges due to, e.g., space or actuation limitations [4]. In the context of minimally invasive surgery (MIS) for instance, the compliance of soft robots might be beneficial for safely navigating around or physically interacting with soft tissue, while increased stiffness might be essential for precise positioning or manipulating tissue, such as cutting or cauterizing [5]–[7]. For an application in this field, an entire manipulator would need to follow requirements with regards to outer dimensions [5].

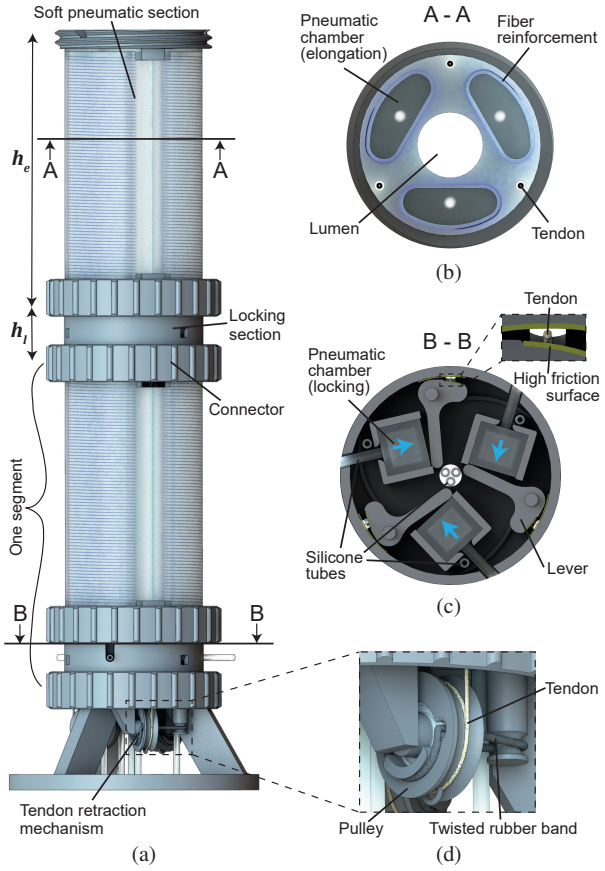

Fig. 1. Soft robotic manipulator, made of two segments/actuators, with integrated antagonistic stiffening based on tendon locking: (a) Overview of the two-segment manipulator. (b) Cross-sectional view showing three fiber-reinforced pneumatic air chambers and channels for three tendons. (c) The locking section can clamp tendons between the outer wall and rigid levers operated by small soft pneumatic chambers. (d) Tendon retraction mechanism: A twisted rubber band ensures each tendon is coiled back onto a pulley as the pneumatic actuation chambers relax.

Many minimally invasive procedures involve medical image guiding, also known as interventional radiology. Due to the non-ionizing radiation and better soft-tissue contrast, more and more minimally invasive procedures are being performed using magnetic resonance imaging, referred to as interventional MRI (iMRI), instead of computed tomography [8]. Examples include tumor biopsy and ablation. Assisting soft robots would require high stiffness for precise needle positioning as well as compliance to enable seamless movement

This work is supported by the Springboard Award of the Academy of Medical Sciences (grant number: SBF003-1109), the Engineering and Physical Sciences Research Council (grant numbers: EP/R037795/1, EP/S014039/1 and EP/V01062X/1), the Royal Academy of Engineering (grant number: IAPP18-19\264), the Deutsche Forschungsgemeinschaft (DFG, grant no. 405030609), and UCL Mechanical Engineering as well as the Dr.-Ing. Erich Müller-Stiftung and the Dr. Jürgen und Irmgard Ulderup Stiftung.

[1]Johann Licher and Helge A. Wurdemann are with the Department of Mechanical Engineering, University College London, UK, e-mail: h.wurdemann@ucl.ac.uk

[2]Johann Licher, Jan Peters and Annika Raatz are with the Institute of Assembly Technology and Robotics, Leibniz University Hannover, Germany, e-mail: peters@match.uni-hannover.de

with the patient's breathing motion during procedures [9], [10]. A soft, variable stiffness robot aimed at procedures in an MRI scanner would also require MR safety, i.e., the use of electrically non-conductive and non-magnetic materials [11].

In recent years, there has been a notable increase in the development of soft robotic actuators, aimed at meeting the demand for variable stiffness. These actuators can be categorized into antagonistic and intrinsic methods of stiffness tuning [4]. Antagonistic methods leverage two opposing forces, inspired by counteracting muscles found in nature [12]. For soft pneumatic manipulators, one force might be generated through air pressure, while the opposing force could be provided by additional pneumatic chambers [13] or tendons actuated by motors [12], [14]. Intrinsic methods, on the other hand, rely on materials with adjustable intrinsic stiffness. For instance, granular jamming and fiber jamming techniques utilize vacuum to induce jamming of particles like coffee powder or multiple fibers of materials such as waxed cotton [15], [16]. Melting-based methods employ low melting point alloys (LMPA), wax, or polymers, often heated by a heating wire [1], [17], [18]. Another technique involves shape memory materials, which can be alloys that return to their preprogrammed initial state upon heating or polymers with a significant drop in elastic modulus when heated above their glass transition temperature [1]. In addition, magneto-rheological materials [19] and electro-rheological materials [20] have been utilized, which typically are fluids whose viscosity increases substantially when subjected to a magnetic or electric field [4]. Some of the aforementioned stiffness mechanisms, e.g., granular jamming [15], fiber jamming [16], tendons [12], and LMPA [21], have been integrated into a soft manipulator with reinforced actuation chambers for minimal invasive surgery (STIFF-FLOP) [15].

When intrinsic stiffness mechanisms are miniaturized or undergo significant deformation or shape change, the variation in stiffness can significantly decrease [17], [22], [23]. Further limitations include only discrete stiffness adjustments [17], [23] and the coupling of the motion and stiffness of the actuator [22]. Antagonistic actuation, on the other hand, offers the potential to achieve high continuous stiffness variation [4], [12]. Employing tendons as one opposing actuation means, proves highly effective due to their material strength. However, when tendons are routed through multiple segments of a continuum manipulator, actuating the tendon to adjust stiffness in a tip segment will affect the configuration of other segments towards the base [24].

This paper presents an antagonistic stiffening mechanism combining pneumatic actuation with tendon locking to achieve configuration- and stiffness control over a wide continuous range of stiffness values. The stiffness increase of our concept does not depend on the volume of any stiffening material and can therefore be miniaturized. [22] Building on our previous work [12], the elongation of a soft pneumatic section, resulting from pneumatic actuation, is opposed by constraining the length of integrated tendons. These tendons are guided inside the soft pneumatic section and can be locked by miniaturized pneumatic chambers, moving rigid levers at the base of the segment. Hence, tendon locking will not affect the configuration of other segments, e.g., situated at the base of a multi-segment robot. One segment with three fiber-reinforced pneumatic actuation chambers and three embedded tendons requires only one proportional regulator (for the soft pneumatic section) and three solenoid valves (for independent tendon locking). In addition, the actuation concept allows MR compatibility and by that potential medical applications under MRI guidance.

Section II describes the new antagonistic stiffening concept as well as the design and manufacturing process of the developed soft manipulator. Section III presents the experimental setup and protocol to evaluate the performance of the new concept. The experimental results using a one- and two-segment manipulator and the assessment of MR compatibility are presented in Section IV, followed by a discussion of the findings in Section V. Section VI reflects on the contribution of this paper.

II. Method, Design, and manufacturing of a tendon-locking actuator

A. Concept of the antagonistic principle

Our antagonistic stiffening mechanism consists of the pneumatic actuation section with three fiber-reinforced chambers and three tendons, that are fixed at the tip with a 120° circumferential displacement and guided along the segment. The tendon-locking mechanism is integrated at the base of each segment (see Fig. 1). Locking is achieved by pressurizing miniaturized pneumatic chambers. Our stiffening mechanism can achieve spatial position and stiffness control while using one proportional regulator and three 3-way solenoid valves per segment. The pressure regulator controls the pressure inside all three air chambers simultaneously, resulting in axial elongation of the actuator. Bending motions are generated by pressurizing the miniaturized pneumatic chambers for tendon locking using the solenoid valves. These locked tendons act as switchable strain-limiting structures translating the axial elongation generated by the elongation section into a bending motion. When a decrease in tendon length is required for a new desired configuration, the pressure inside the soft pneumatic section will need to be reduced first, to shorten the segment and retract the tendon. The tendon must then be locked again before advancing toward the new configuration through pressurization. A tendon retraction mechanism is integrated at the bottom to prevent tendon buckling while the soft body retracts. Multiple segments each consisting of a soft pneumatic and a locking section, can be combined into a soft robotic arm.

Antagonistic stiffening results from two counteracting forces, e.g., by locking all three tendons in their position and pressurizing the air chambers of the soft robot. The continuous control of the elongation pressure using a proportional regulator results in a continuous adaptability of the stiffness.

B. Fabrication of the soft pneumatic section

The design and manufacturing process of the soft pneumatic section is adapted from work by Shi et al. [25]. The

design of three semi-circular chambers (see Fig. 1 (b)) was chosen due to an improved actuation efficiency and larger workspace compared to circular shaped cross-sections [25]. Note, that the soft pneumatic section in this paper is larger (Fig. 2), as it simplified the proof-of-concept of the stiffening mechanism and is better suited for the assistance of interventions under MRI [9].

The fabrication procedure of one soft section is shown in Fig. 3. First, the inextensible fiber reinforcement is prepared for each actuation chamber. Then, the main body is molded from Smooth-On Ecoflex 00-50 (EF 50), while the top and bottom caps are molded from Smooth-On Dragon Skin 30 (DS 30). To guide the tendons along the segment and prevent them from cutting into the silicone, silicone tubes (Altec AlteSil OD 2 mm, ID 1 mm) are integrated. Another set of silicone tubes for the connection to the actuation chambers is inserted using silicone glue (Wacker Elastosil E41). Lastly, 3D-printed connectors (Formlabs Tough 2000) are attached at the top and bottom of the silicone body using Loctite Superglue to be able to secure the tendons (McMaster-Carr High-Strength High-Temperature Thread 0.014") at the tip and ease the connection to other sections of the segment.

C. Design and manufacturing of the tendon locking section

The locking section of the actuator is designed to constrain/lock or release tendon movement, during pressurization of the soft pneumatic section. Hence, the tendon forces, required to constrain the tendon when the soft pneumatic section is elongated were tested by attaching it to a solid base and measuring the tendon force (force/torque sensor IIT FT-17) while applying the actuation pressure to the elongation chambers. As shown in the supplementary video the maximum tendon force measured at 80 kPa is 13.64 ± 0.02 N for one locked tendon and 15.93 ± 0.10 N for two locked tendons. These values serve as requirements for the locking mechanism.

One effective actuation method to lock tendons offers air pressure, which is in line with the actuation type of the soft pneumatic section. Based on a thorough experimental comparison of different pneumatically activated locking

A_c	172.5	mm^2	d_1	16	mm	d_2	40.6	mm	d_l	4.5	mm
d_c	9	mm	D_1	44	mm	d_m	9	mm	D_2	48	mm
δ_f	1	mm	h_e	88	mm	δ_m	1.5	mm	h_l	17	mm
r_t	19.8	mm	w_c	22.9	mm	w_m	10	mm			

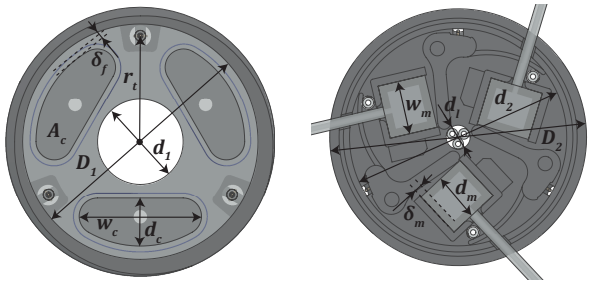

Fig. 2. Design dimensions of the soft, soft pneumatic section (left figure) and locking mechanism (right figure). Some dimensions are shown in Fig.1.

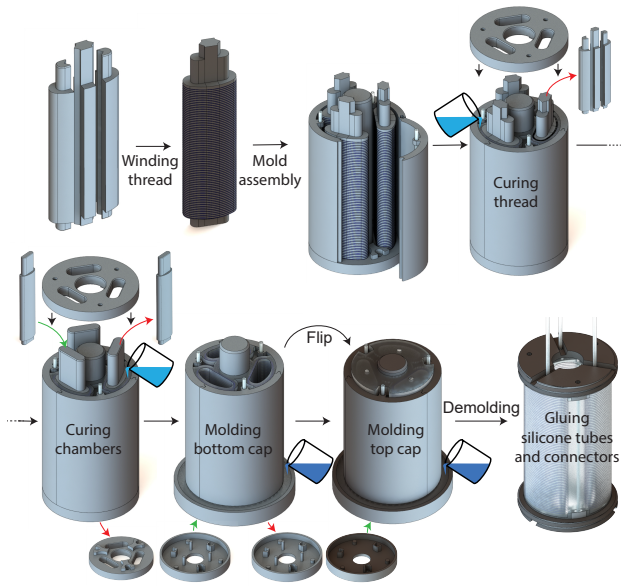

Fig. 3. Molding process of the pneumatically actuated robot: Inextensible thread is wound around the actuation chamber rods like a screw thread. Together with silicone tubes, that will guide tendons, the actuation chamber rods are positioned into a cylindrical mold, that is then filled in with EF 50 silicone. Once the silicone is cured and the actuation chamber rods are removed, silicone is poured into the actuation chambers, and narrower chamber rods are inserted. The bottom and top of the segment are sealed with a cap of DS 30 silicone. After demolding, silicone tubes for pneumatic actuation as well as two 3D-printed connectors are glued to the body.

mechanisms (see supplementary video), it was decided to create miniaturized rectangular pneumatic chambers molded from silicone (Smooth-On Dragon Skin 20) to move small levers. This mechanism, shown in Fig. 1 (c), is inspired by Wei et al. [26]. When a pneumatic locking chamber is pressurized, a minimal rotational motion of the lever results in clamping the tendon between the surfaces of the other end of the lever and the inner wall. These surfaces are covered with sandpaper (grit P240), increasing the friction between the clamping surfaces and the tendons. The levers are equipped with rotational springs to ensure that the levers return to their initial position in the unlocked state. The main body, cap, and levers are all 3D printed using Formlabs Tough 2000 resin. The dimensions are included in Fig. 2. This mechanism can achieve tendon forces of 26.65 ± 2.23 N at a pressure of 200 kPa inside the small chambers. This exceeds the required force to bend the elongation section by at least 10.72 N.

D. Integration of a tendon retraction mechanism

To allow a decrease in length of an unlocked tendon without buckling, when the pressure in the soft pneumatic section is reduced, a system has been created that applies a consistent force to one side of the tendon. The system features the tendon wound around a pulley on an MR-safe bearing (igus BB-684-B180-30-GL). The pulley is pre-tensioned, using a twisted rubber band spring (O-ring 15.5 mm $\times$ 1.5 mm) as shown in Fig. 1 (d). These components were 3D printed using Formlabs Tough 2000 resin. Modularity is achieved through

a connector that ensures concentric alignment and inhibits both rotation and axial displacement.

III. Experimental Setup and Protocol

A. Experimental setup

For our experiments, we utilized the characterization and control platform for pneumatically driven soft robots developed by Shi et al. [27]. The pressure in the elongation and locking chambers was controlled using four Camozzi K8P proportional pressure regulators (Note: For the locking chambers, 3-way solenoid valves would be sufficient). The position and orientation of the actuator tip were measured using a 6 DoF electromagnetic tracker (NDI Aurora). For stiffness characterization, a linear rail (Zaber X-LSM100A) equipped with a force/torque sensor (IIT FT-17) was used to measure both force values and deflection (see Fig. 5 (c)).

B. Experimental protocol

1) Experiment 1 - Reachable workspace: This experiment focused on understanding the positions of the tip that can be reached by one robotic segment influenced by different pressure values in the soft pneumatic section and the clamping length of each tendon. Hence, the pressure in the soft pneumatic section were varied up to 80 kPa with a resolution of 20 kPa. The pressure values in the clamping chambers were set to either 0 kPa (unlocked) or the maximum of 300 kPa (locked).This new type of actuation is called Tendon-Locking (TL) actuation in the following. All combinations of locking-activation pressure values determining the length of the three tendons were set for every final elongation pressure value, resulting in 225 combinations. In addition, we carried out experiments to compare the workspace with the manipulator actuated with air pressure in each chamber independently, in line with [25]. This actuation type with removed tendons is from now on referred to as Purely Pneumatic (PP) actuation. Here the same pressure values were applied.

2) Experiment 2 - Bending angle: Firstly, the bending angle was measured for TL-actuation with a maximum pressure in the soft pneumatic section of 80 kPa and 20 kPa pressure steps while locking one or two tendons. We compared these measurements with the bending angles that were achieved by PP-actuation when pressurizing one or two chambers of the soft pneumatic section with the same pressure values.

3) Experiment 3 - Stiffness characterization: First, force-deflection curves were measured for TL-actuation. A displacement of 10 mm was applied before and after stiffening by locking all tendons and applying an additional pressure of 20 kPa to the soft pneumatic section. Second, the stiffness of a PP-actuated section was analyzed for comparison. All tendons were removed for this part of the experiment. Three configurations were chosen as shown in Fig. 5. In configuration (a), the segment is elongated by 20 mm and the tip is deflected laterally by 10 mm. In configurations (b) and (c), the segment is set to a 75° bending angle and the tip is deflected 10 mm perpendicular to the bending plane (b) and within the bending plane (c). For the PP-actuation, only one chamber of the soft pneumatic section was pressurized to achieve bending. For TL-actuation, one tendon was locked to bend the segment.

4) Experiment 4 - Independent stiffness control for a two-segment manipulator: To demonstrate that the stiffness of each segment in a multi-segment manipulator can be controlled individually, we measured the stiffness of a two-segment robot at the tip of the base segment and the tip of the overall manipulator. First, only the base segment was stiffened by locking all tendons and applying an additional pressure of 20 kPa to the soft pneumatic section. Then, both segments were stiffened in the same way. Stiffness was measured by pulling on a thread fixed to the tip of each segment. This thread was tied to the force sensor which was moved using the linear rail as shown in Fig. 5 (c). In this way, the forces were measured during a deflection of 10 mm.

IV. Experimental Results

A. Results for Experiment 1 - Reachable workspace

The workspaces for TL-actuation (blue color) and PP-actuation (orange color) shown in Fig. 4 (a) are dome-shaped. The workspace for PP-actuation extends over the range $[-82.15, 63.77]$ mm in x-, $[-65.54, 80.75]$ mm in y-, and $[43.45, 140.65]$ mm in z-direction. For the TL-actuation, the workspace reaches $[-87.66, 73.68]$ mm, $[-83.57, 81.65]$ mm, and $[41.06, 139.71]$ mm in x-, y-, and z-direction. In the xy-plane a maximum deflection between 56.48 mm and 89.17 mm is achievable depending on the radial direction when using PP-actuation. For our proposed system the maximum radial deflection varies between 69.51 mm and 91.42 mm. The difference lowers by 33.0 %, resulting in a higher radial uniformity of the workspace. The workspace volume was calculated to be 437.2 cm^3 for PP-actuation and 526.2 cm^3 for our concept, i.e., an increase of 20.4%.

B. Results for Experiment 2 - Bending angle

Fig. 4 (b) shows the bending angles versus actuation pressure for PP-actuation of one or two chambers (orange color) and TL-actuation with one or two tendons locked (blue color). All curves show a nonlinear increase for pressure values below 60 kPa. For higher pressures, they behave almost linearly. The curves of the bending angles for one and two clamped tendons as well as two-chamber PP-actuation almost overlap up to 60 kPa. The bending angles for one pressurized pneumatic chamber are well below the other actuation modes with a maximum bending angle of $83.4 \pm 2.4°$ at 80 kPa pressure. Our proposed actuation concept (one locked tendon) achieves $121.3 \pm 3.1°$ at 80 kPa in the same radial direction, an improvement of 45.4 %. The maximum bending angle for PP-actuation of $139.4 \pm 6.5°$ can be achieved by pressurizing two chambers with 80 kPa. The maximum achievable bending angle for tendon-locking actuation of $143.6 \pm 3.9°$ at 80 kPa is not significantly different. Hence, the difference between the two radial directions lowers by 60.2 %, resulting in a more uniform workspace.

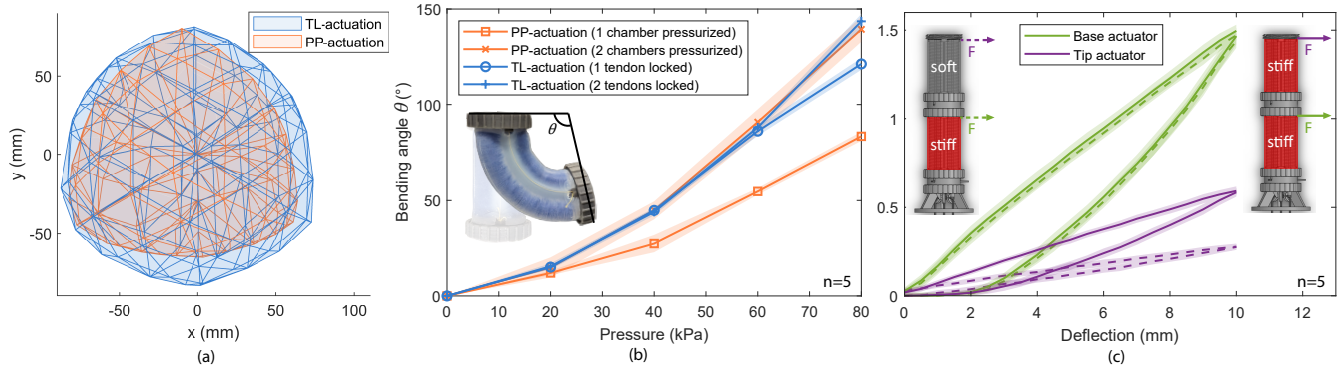

Fig. 4. (a) Results for Experiment 1: Workspace for one segment using TL-actuation and PP-actuation in the x-y-plane. (b) Results for Experiment 2: Bending angles for different actuation pressures up to 80 kPa. The curves for the TL-actuation with one (o) and two locked tendons (+) are shown in blue; PP-actuation using one (*) and two chambers (x) in orange color. Note: All elongation chambers are pressurized equally for bending using TL-actuation. (c) Results for Experiment 4: Force-deflection curves for configurations, stiffening only the base segment (dashed line) and both segments (continuous line). The forces needed for deflection were measured at the tip of the base segment (green color) and at the very tip of the manipulator (purple color).

C. Results for Experiment 3 - Stiffness characterization

Fig. 5 shows that stiffness values for the TL-actuation without stiffening are similar for configurations (a) and (b). With active stiffening, i.e., tendons are locked and an additional pressure value of 20 kPa is added, the stiffness in (a) increases by 201.7 % from 0.0480 ± 0.0017 N/mm to 0.145 ± 0.0028 N/mm. At the same time, the dissipated energy, which characterizes the hysteresis, increases from 1.04 mJ to 2.72 mJ. For configuration (b), the stiffness of the TL-actuation increases by 138.0 % from 0.0542 ± 0.0031 N/mm to 0.129 ± 0.0030 N/mm upon stiffening. The dissipated energy rises less than for configuration (a), increasing from 1.11 mJ to 1.28 mJ. For configuration (c), it is noticeable that the curves for the tendon-locking actuation fluctuate. The stiffness, when using the TL-actuation without stiffening (0.338 ± 0.0206 N/mm) is larger than the stiffness for PP-actuation (0.307 ± 0.0166 N/mm). When the stiffening is activated, the stiffness increases by 23.4 % to 0.417 ± 0.0195 N/mm. The dissipated energy is significantly larger when using TL-actuation without (10.67 mJ) and with (12.90 mJ) stiffening compared to PP-actuation (3.83 mJ).

D. Results for Experiment 4 - Independent stiffness control for a two-segment manipulator

Fig. 4 (c) shows the force-deflection curves for a two-segment manipulator when stiffening one and two segments, respectively. The results compare stiffness measured when pulling the tip of the base segment and the tip segment. The stiffness value for the base actuator is 0.1472 ± 0.0029 N/mm with a soft tip segment and 0.1496 ± 0.0035 N/mm with a stiffened tip segment. The stiffness value at the tip segment increases by 113.3 % from 0.0278 ± 0.0017 N/mm to 0.0593 ± 0.0027 N/mm upon stiffening.

E. MR-compatibility assessment

For some medical applications, MR compatibility of the manipulator is a mandatory requirement [11]. To understand the level of distortion and signal loss artifacts occurring in MRI [28], the loss of signal-to-noise ratio (SNR) was determined according to the NEMA MS 1-2008 standards (Method 4) [29]. MR images were captured using a Siemens MAGNETOM Aera with a magnetic field strength of 1.5 T. For the reference scan, we used an artificial phantom filled with an MRI filling solution. For the second scan, the manipulator was placed next to the phantom inside the area of interest to prove zone 1 MR compatibility [30]. As shown in the supplementary video the manipulator is visible in the MR scan without resulting in significant artifacts. Comparing the two MR images, the SNRs have been calculated to 18.53 dB and 18.51 dB, i.e., an SNR loss of 0.36 %.

V. Discussion

In Exp. 1 to 3, our proposed TL-actuation has been compared to PP-actuation. Exp. 2 shows that our antagonistic actuation principle can achieve maximum bending angles of similar values for locking one or two tendons. Comparing these results to PP-actuation, one-chamber actuation only achieves about 60% of the bending angle resulting from two-chamber actuation. A reason for this difference in bending behavior might be that our approach pressurizes all three chambers equally, instead of only one or two chambers, resulting in substantially higher forces. This feature also results in a larger, more uniform workspace shown in Exp. 1.

The stiffness increase in Exp. 3 for our approach results from increased opposing forces when tendons are locked and additional pressure is added. The tensioned tendons with high stiffness transfer the applied forces along the segment to the base. This effect depends on the configuration, causing the variation of stiffness increases for configurations (a),(b), and (c). At the same time, the hysteresis grows when stiffening is activated due to friction between the tendons and the guiding silicone tubes as well as larger internal friction in the silicone due to larger pressure values. The force fluctuation visible for configuration (c), results from observable stick-slip motions between the force sensor and the tip cap of the segment.

Exp. 4 proves that our stiffening principle affects a single segment without influencing the stiffness of other segments for multi-segment manipulators, as the locking mechanism

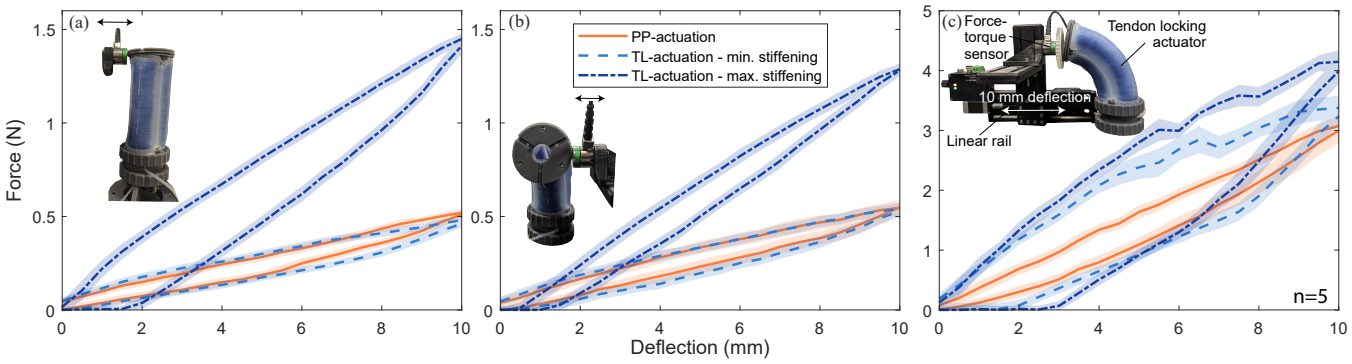

Fig. 5. Results for Experiment 3: Force-deflection curves for configurations (a), (b), and (c) comparing PP-actuation and the TL-actuation with and without stiffening. Note that the scaling of the y-axis in (a) and (b) is different from (c).

is placed at the bottom of each segment. Hence, the stiffness measured at the tip of the base segment does not change when the tip segment is stiffened in Fig. 4 (c).

The visibility of the silicone in the MR image must be attributed to the presence of hydrogen atoms in the material. Most importantly, our manipulator does not result in significant artifacts or obstruct the view of any target, thanks to the MR scanner's 3D imaging capabilities. Instead, the visibility aids in understanding the manipulator's pose.

One of the limitations of our actuation concept results from locking the tendons instead of pulling them with motors, preventing the actuator from moving to configurations with smaller tendon lengths without depressurization. This limits the trajectories it can follow. However, for multi-segment manipulators, arbitrary trajectories could be tracked by using motors to pull the tendons at the base segment while using the proposed locking concept for the other segments. Another limitation is the potential delay in actuation within MR environments - a consequence of the long silicone tubes required by the placement of non-MR-compatible valves at a distance from the scanner. After more than 100 tests, no harm to the tendons could be detected. However, the durability should be proven by further tests.

Table I compares our antagonistic stiffening concept with other methods, that offer similar actuation capabilities, in particular, spacial position control. It is worth noting that a comparison presents challenges due to variations in designs, dimensions, test configurations and stiffening metrics. In this section, we use the scale-invariant stiffness increase as the benchmark. The table shows that our design results in a significantly higher stiffness increase for configurations (a) and (b) (Fig.5), compared to the tendon and pneumatic stiffening methods introduced in [12] and the granular stiffening approach utilized in [15]. The stiffness increase for configuration (c) remains almost unchanged. When compared to the fiber jamming actuator proposed by Brancadoro et al. [16], our segment shows a notably higher stiffness range for configurations (a) and (c). The LMPA stiffening concept [21], while achieving a larger stiffness range than our technique, is significantly slower and lacks MR compatibility.

TABLE I

COMPARISON OF STIFFNESS CAPABILITY WITH CURRENT METHODS

Stiffening concept	**Achievable stiffness increase**		
	Config. (a)	**Config. (b)**	**Config. (c)**
Granular jamming [15]	36 %	19.6 %*	17.2 %*
Fiber jamming (Module A) [16]	22 ± 15 %	-	no significant**
LMPA [21]	450 ± 52 %	-	393 ± 55 %**
Tendon + pneumatic (motor) [12]	69.1 %	30.7 %*	24.3 %*
Tendon locking (our method)	201.7 %	138.0 %	23.4 %

* bending angle of 90° ** bending angle of about 40°

VI. CONCLUSIONS

This paper presents a new antagonistic stiffening mechanism that combines pneumatic actuation with switchable strain-limiting structures, facilitating control over both configuration and stiffness. The elongation, introduced by inflating a soft pneumatic section, is counteracted by constraining the movement of integrated tendons through a locking mechanism. This approach enables a segment to achieve bending angles up to 143.6° while allowing for stiffness adjustments up to a 201.7 % increase. The actuation concept provides a larger and more consistent workspace in comparison to traditional methods, which rely on the pneumatic actuation of three individual pneumatic chambers, as well as enhances the range of stiffness values achievable beyond that of existing stiffening methods. Furthermore, the experimental results demonstrate the potential of this actuation concept in enabling selective stiffening of individual segments within multi-segment robots, while maintaining MR compatibility.

Future work will include miniaturization of the tendon locking mechanism, which we consider feasible using manufacturing methods like CNC-milling and the combination with a sub-10 mm soft pneumatic section required for some potential applications in the medical field, e.g. minimally invasive surgery. Here, combinations of motor-driven tendon actuation and segment-specific stiffness control will be explored. Overall, we like to investigate to what extent modeling frameworks for kinematics and stiffness analysis will be applicable to our antagonistic stiffening principle.

ACKNOWLEDGMENT

The authors like to thank Prof. Vivek Muthurangu and Mr Yaxi Wang for their support during MR-compatibility testing.

REFERENCES

[1] Y. Yang, Y. Li, and Y. Chen, "Principles and methods for stiffness modulation in soft robot design and development," *Bio-Design and Manufacturing*, vol. 1(1), pp. 14–25, 2018.

[2] E. W. Hawkes, C. Majidi, and M. T. Tolley, "Hard questions for soft robotics," *Science Robotics*, vol. 6(53), p. eabg6049, 2021.

[3] J. Shi, A. Shariati, S.-A. Abad, Y. Liu, J. S. Dai, and H. A. Wurdemann, "Stiffness modelling and analysis of soft fluidic-driven robots using Lie theory," *The International Journal of Robotics Research*, vol. 43(3), pp. 354–384, 2024.

[4] M. Manti, V. Cacucciolo, and M. Cianchetti, "Stiffening in Soft Robotics: A Review of the State of the Art," *IEEE Robotics & Automation Magazine*, vol. 23(3), pp. 93–106, 2016.

[5] J. Zhu, L. Lyu, Y. Xu, H. Liang, X. Zhang, H. Ding, and Z. Wu, "Intelligent Soft Surgical Robots for Next-Generation Minimally Invasive Surgery," *Advanced Intelligent Systems*, vol. 3, 2021.

[6] S.-A. Abad, A. Arezzo, S. Homer-Vanniasinkam, and H. Wurdemann, "Soft robotic systems for endoscopic interventions," *Endorobotics*, pp. 61–93, 2022.

[7] K.-W. Kwok, H. Wurdemann, A. Arezzo, A. Menciassi, and K. Althoefer, "Soft robot-assisted minimally invasive surgery and interventions: Advances and outlook," *Proceedings of the IEEE*, vol. 110(7), pp. 871–892, 2022.

[8] J. Barkhausen, T. Kahn, G. Krombach, C. Kuhl, J. Lotz, D. Maintz, J. Ricke, S. Schönberg, T. Vogl, and F. Wacker, "White Paper: Interventional MRI: Current Status and Potential for Development Considering Economic Perspectives, Part 1: General Application," *RöFo - Fortschritte auf dem Gebiet der Röntgenstrahlen und der bildgebenden Verfahren*, vol. 189(7), pp. 611–623, 2017.

[9] K. Schlockermann, J. Peters, B. Hensen, J. J. Löning C., F. Wacker, and A. Raatz, "Soft Robot Assistance for Tumor Biopsy and Ablation in Magnetic Resonance Imaging," *New Trends in Medical and Service Robotics*, pp. 3–12, 2023.

[10] J. Peters, J. Licher, B. Hensen, F. Wacker, and A. Raatz, "Soft Robotic Actuator Leveraging Switchable Strain-Limiting Structures for Tumor Biopsy and Ablation in MRI," in *IEEE International Conference on Soft Robotics*, 2024, pp. 983–989.

[11] D. Stoianovici, C. Kim, D. Petrisor, C. Jun, S. Lim, M. W. Ball, A. Ross, K. J. Macura, and M. E. Allaf, "MR Safe Robot, FDA Clearance, Safety and Feasibility of Prostate Biopsy Clinical Trial," *IEEE/ASME Transactions on Mechatronics*, vol. 22(1), pp. 115–126, 2017.

[12] A. Shiva, A. Stilli, Y. Noh, A. Faragasso, I. D. Falco, G. Gerboni, M. Cianchetti, A. Menciassi, K. Althoefer, and H. A. Wurdemann, "Tendon-Based Stiffening for a Pneumatically Actuated Soft Manipulator," *IEEE Robotics and Automation Letters*, vol. 1(2), pp. 632–637, 2016.

[13] S. P. M. Babu, A. Sadeghi, A. Mondini, and B. Mazzolai, "Antagonistic Pneumatic Actuators with Variable Stiffness for Soft Robotic Applications," *IEEE International Conference on Soft Robotics*, pp. 283–288, 2019.

[14] L. Manfredi, L. Yue, J. Zhang, and A. Cuschieri, "A 4 DOFs variable stiffness soft module," *IEEE International Conference on Soft Robotics*, pp. 94–99, 2018.

[15] M. Cianchetti, T. Ranzani, G. Gerboni, I. De Falco, C. Laschi, and A. Menciassi, "STIFF-FLOP surgical manipulator: Mechanical design and experimental characterization of the single module," *International Conference on Intelligent Robots and Systems*, pp. 3576–3581, 2013.

[16] M. Brancadoro, M. Manti, F. Grani, S. Tognarelli, A. Menciassi, and M. Cianchetti, "Toward a Variable Stiffness Surgical Manipulator Based on Fiber Jamming Transition," *Frontiers in Robotics and AI*, vol. 6, 2019.

[17] J. Peters, E. Nolan, M. Wiese, M. Miodownik, S. Spurgeon, A. Arezzo, A. Raatz, and H. A. Wurdemann, "Actuation and stiffening in fluid-driven soft robots using low-melting-point material," *IEEE/RSJ International Conference on Intelligent Robots and Systems*, pp. 4692–4698, 2019.

[18] J. Peters, C. M. Sourkounis, M. Wiese, T. Kwasnitschka, and A. Raatz, "Single Channel Soft Robotic Actuator Leveraging Switchable Strain-Limiting Structures for Deep-Sea Suction Sampling," *IEEE/RSJ International Conference on Intelligent Robots and Systems*, pp. 6484–6490, 2023.

[19] M. A. Moreno-Mateos, M. Hossain, P. Steinmann, and D. Garcia-Gonzalez, "Hybrid magnetorheological elastomers enable versatile soft actuators," *npj Computational Materials*, vol. 8(1), pp. 1–14, 2022.

[20] A. Sadeghi, L. Beccai, and B. Mazzolai, "Innovative soft robots based on electro-rheological fluids," *IEEE/RSJ International Conference on Intelligent Robots and Systems*, pp. 4237–4242, 2012.

[21] N. Pagliarani, L. Arleo, S. Albini, and M. Cianchetti, "Variable Stiffness Technologies for Soft Robotics: A Comparative Approach for the STIFF-FLOP Manipulator," *Actuators*, vol. 12(3), p. 96, 2023.

[22] W. Dou, G. Zhong, J. Cao, Z. Shi, B. Peng, and L. Jiang, "Soft Robotic Manipulators: Designs, Actuation, Stiffness Tuning, and Sensing," *Advanced Materials Technologies*, vol. 6(9), p. 2100018, 2021.

[23] J. Konstantinova, H. Wurdemann, A. Shafti, A. Shiva, and K. Althoefer, *Soft and Stiffness-controllable Robotics Solutions for Minimally Invasive Surgery: The STIFF-FLOP Approach*. River Publishers, 2018.

[24] J. Lai, B. Lu, and H. K. Chu, "Variable-Stiffness Control of a Dual-Segment Soft Robot Using Depth Vision," *IEEE/ASME Transactions on Mechatronics*, vol. 27(2), pp. 1034–1045, 2022.

[25] J. Shi, W. Gaozhang, and H. Wurdemann, "Design and Characterisation of Cross-sectional Geometries for Soft Robotic Manipulators with Fibre-reinforced Chambers," *IEEE International Conference on Soft Robotics*, pp. 125–131, 2022.

[26] D. Wei, T. Gao, X. Mo, R. Xi, and C. Zhou, "Flexible Bio-tensegrity Manipulator with Multi-degree of Freedom and Variable Structure," *Chinese Journal of Mechanical Engineering*, vol. 33(1), p. 3, 2020.

[27] J. Shi, W. Gaozhang, H. Jin, G. Shi, and H. Wurdemann, "Characterisation and control platform for pneumatically driven soft robots: Design and applications," *IEEE International Conference on Soft Robotics*, pp. 1–8, 2023.

[28] ASTM, "ASTM F2503-20: Standard Practice for Marking Medical Devices and Other Items for Safety in the Magnetic Resonance Environment," 2020.

[29] NEMA, "NEMA MS 1-2008: Determination of Signal-to-Noise Ratio (SNR) in Diagnostic Magnetic Resonance Imaging," 2021.

[30] N. Yu and R. Riener, "Review on MR-Compatible Robotic Systems," *International Conference on Biomedical Robotics and Biomechatronics*, pp. 661–665, 2006.